Computational model of retinal photocoagulation and rupture

Christopher Sramek[*1], Yannis M. Paulus[2], Hiroyuki Nomoto[2], Phil Huie[2,3], Daniel Palanker[2, 3]

[1]Department of Applied Physics, [2]Department of Ophthalmology, [3]Hansen Experimental Physics Laboratory,
Stanford University, Stanford, CA

ABSTRACT

In patterned scanning laser photocoagulation, shorter duration (< 20 ms) pulses help reduce thermal damage beyond the photoreceptor layer, decrease treatment time and minimize pain. However, safe therapeutic window (defined as the ratio of rupture threshold power to that of light coagulation) decreases for shorter exposures. To quantify the extent of thermal damage in the retina, and maximize the therapeutic window, we developed a computational model of retinal photocoagulation and rupture. Model parameters were adjusted to match measured thresholds of vaporization, coagulation, and retinal pigment epithelial (RPE) damage. Computed lesion width agreed with histological measurements in a wide range of pulse durations and power. Application of ring-shaped beam profile was predicted to double the therapeutic window width for exposures in the range of 1 – 10 ms.

Keywords: photocoagulation, damage threshold, computer model, retinal thermal damage

1. INTRODUCTION

Since its introduction nearly 40 years ago, laser photocoagulation has become the standard of care for long-term therapy of various retinopathies [1-4]. Typically, spot sizes of 50 – 500 μm and durations of 100 – 500 ms have been used. Pulses of these durations coagulate the photoreceptor layer, but lack selectivity, as they are known to damage the inner retina [5]. Recently introduced Patterned Scanning Laser photocoagulation greatly simplifies and accelerates the procedure by delivering a pattern of multiple retinal lesions in a single step [6]. A scanning laser is used to apply 4 to 50 lesions, 10 to 30 ms in duration, with the total number of pulses limited by the eye fixation time. Short duration (< 20 ms) pulses have been found beneficial for reducing thermal damage beyond the photoreceptor layer, decreasing treatment time and minimizing pain while maintaining efficacy [5, 7, 8]. However, coagulation with shorter pulses requires higher peak temperatures, increasing the potential for retinal rupture and reducing the therapeutic window (defined as the ratio of power for producing a rupture to that of light coagulation) [9]. The safe therapeutic window decreases for decreasing pulse duration and has been reported to be between 2.5 and 3 for 10 ms pulses [10].

It is desirable to implement photocoagulation with shorter pulses in order to increase the number of lesions in a single pattern. At the same time, the safety margin should decrease below 3, as pigmentation in human fundus varies by about a factor of 2-2.5 [11, 12]. It is thus useful to understand the variation of the peak temperature and spatial extent of thermal damage with pigmentation, power and duration of exposure. Computational thermal modeling can help in this regard, as it allows for the estimation of temperature elevation within the retina during and after the laser pulse. Coupling the evolution of hyperthermia in tissue with a thermal model of cellular damage allows for the prediction of lesion size for arbitrary pulse parameters. Ability to compute the expected lesion size and safety range allows for optimization of the treatment parameters for short laser pulses. Typically, models for retinal photocoagulation numerically solve the heat conduction equation and estimate the damage extent using the Arrhenius rate process model for cellular death [13-20]. However, none of the existing models incorporate retinal rupture, an integral

[*] csramek@stanford.edu; phone 1 650 723-0130; http://www.stanford.edu/~palanker/lab/

factor for describing the safety limits of photocoagulation and an important process for a clinically relevant model of short pulse treatments.

Two model parameters are critical for a retinal photocoagulation model capable of making quantitative predictions: (a) accurate description of the beam geometry and absorption characteristics of the pigmented tissues, and (b) determination of the activation energy in the Arrhenius damage model. Variations in heat deposition directly affect the temperature rise during the laser pulse, which is a key for two reasons. First, the exponential dependence of cell death on temperature in the Arrhenius damage model means that small changes in temperature can have a large impact on the extent of damage. Second, rupture occurs due to vaporization of intracellular water and expansion of a resulting vapor bubble [21]. Vaporization thus provides both an upper bound on temperature and a standard for calibrating the absolute temperature rise. Variability in heat deposition can arise from many sources: speckling, focusing errors, optical aberrations, and variations in RPE pigmentation. Melanosome density varies across the RPE cell and from cell-to-cell [22]. The degree of non-uniformity in RPE pigmentation varies between species, but variations as high as a factor of three from macula to periphery have been reported [23]. These factors can act as "hot spots" with higher corresponding peak temperature in areas of higher irradiance or optical absorption, which may start vaporization.

The Arrhenius model describes protein denaturation with an exponential dependence of the reaction rate on temperature, and quantifies the change in a critical component of cellular viability with the integral:

$$\Omega_{threshold} = A\int_0^{\tau} \exp\left(-\frac{E^*}{R_u T(t)}\right)dt \qquad (1)$$

where E* is the activation energy (J/mol), A is the rate constant (1/s), R is the gas constant (8.32 J/mole-K), T is the absolute temperature (K), and τ is the duration of hyperthermia (s). An Arrhenius integral of unity corresponds to a factor of *e* decrease in concentration of this component and is generally taken as the threshold for cell death. This model has been described in detail elsewhere [24, 25]. Protein denaturation activation energies have been measured between 200 and 800 kJ/mol [15]. Porcine corneal damage has been described with an activation energy of 106 kJ/mol and cultured NIH3T3 cells were estimated to have an activation energy of 96 kJ/mol [25, 26]. An activation energy of 290 kJ/mol was inferred from millisecond argon laser lesions in retina, a value which has been commonly used in photocoagulation models [27]. In this work, an independent measurement of this model parameter was made, as well as measurements of laser irradiance and absorption coefficient distribution in tissue. A thermal damage model was constructed based on these measurements and was used for computing the lesion width and safe therapeutic window for different treatment parameters.

2. MATERIALS AND METHODS

2.1 Laser system

A 532 nm CW Nd:YAG laser system (PASCAL, Optimedica, Santa Clara, CA) was used in this study. The system telecentrically images the surface of a multimode fiber through a scanning system and provides 1 – 200 ms duration pulses with peak output power between 10 and 2500 mW. A foot pedal activates the laser, and a graphic user interface allows for control over power, spot size and pulse duration. The 200 μm fiber was selected in these experiments. In the aerial focal plane, the intensity was nominally top-hat with the intensity transition from 10% to 90% occurring over roughly 20 μm. Intensity fluctuations due to speckling were approximately ±20%. For 1 ms pulses, these fluctuations are calculated to produce only small changes (~5%) in local peak temperature, and even smaller variations for longer durations.

2.2 RPE absorption and pigmentation variability

RPE sheets were extracted from three Dutch Belted rabbit eyes 30 minutes post-enucleation. Square sections of posterior pole were excised and the retina was peeled away from each, with sheets of RPE adhering to the neural retina intact. The retinas (~4 mm^2 in area) were placed in fixative and examined with transmission microscopy, using a 563 nm wavelength LED (B4303F5, CML Innovative Technologies, Inc., Hackensack, NJ) for illumination. A CCD camera (Micropublisher 3.3; Qimaging Inc., Surrey, BC) was used to acquire images of RPE cells, with a 50 μm metal wire placed in the sample plane as a dark reference level. The *ImageJ* software package was used to estimate cell-to-cell variation in RPE absorption

[28]. A grayscale threshold was applied to binarize each image and outline the boundaries between the pigmented regions (N = 1623 regions total). For each fitted region, the green channel grayscale value and the area were recorded.

2.3 Vaporization in the RPE explants

An optical system was used to monitor transmission and backscattering of laser light during the irradiation of RPE explants (Figure 1). Samples were prepared from 1-day-old porcine eyes, shipped on ice overnight after enucleation. Eyes were cut equatorially, and the anterior pole and vitreous humor were removed. Square samples (~200 mm^2 in area) were prepared from the posterior pole of each eye and the neural retina was peeled away.

Samples were irradiated at fixed power levels from 160 to 640 mW. A large area photodiode (2031; New Focus, Inc., San Jose, CA) measured transmission through the sample, while a second photodiode (DET410, Thorlabs, Inc., Newton, NJ) measured the backscattered light through a beamsplitter. A digital oscilloscope (model TDS1001B, Tektronix, Inc., Beaverton, OR) recorded the characteristic peaks corresponding to bubble formation from both detectors. Pulse length was varied with power to ensure that a vaporization signal was observed for all power levels. The time delay between pulse onset and peak maximum was recorded for each exposure (11 eyes, 3300 total exposures).

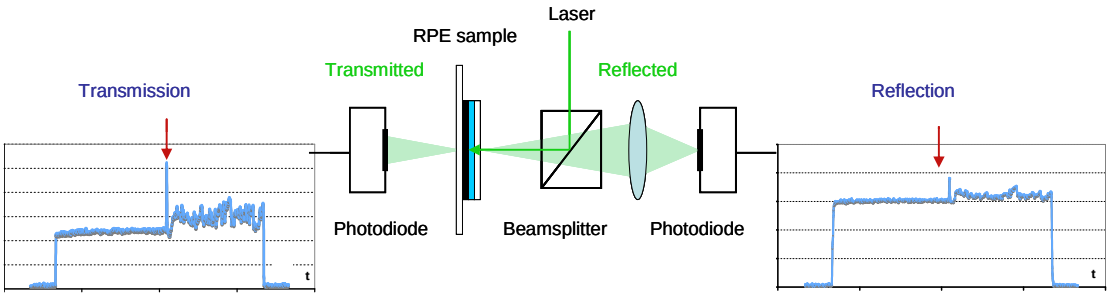

Fig. 1. Experimental setup for vaporization delay measurement. Delay was measured between the pulse onset and the first peak maximum for 6 incident powers between 160 and 640 mW.

2.4 Beam shape and power transmission in the eye

Beam shape and power in the retinal plane were measured in the rabbit eyes. A single eye was enucleated from each of 3 rabbits, one Dutch Belted and two New Zealand Whites. A 4 mm hole was trepanized through the posterior pole in the macular region. A microscope glass cover was glued over the posterior pole to cover the hole and maintain the globe integrity and intraocular pressure. A laser contact lens (OMSRA-S; Ocular Instruments, Bellevue, WA) focused the laser beam onto the cover slip. A 300 µm grid transparency served as a target for focusing the laser and calibrating the beam images at the retinal plane. An imaging objective lens (10×) magnified the beam in the retinal plane onto a CCD (Micropublisher 3.3; Qimaging Inc., Surrey, BC) and power meter head (PD-300; Ophir Optonics Ltd, Jerusalem, Israel). An iris restricted imaging and power to a 500 µm diameter in the retinal plane.

2.5 RPE viability

Seven Dutch Belted rabbits were used in accordance with the Resolution of the Association for Research in Vision and Ophthalmology, and with approval from the Stanford University Animal Institutional Review Board. The rabbits were each anesthetized and a laser contact lens (OMSRA-S; Ocular Instruments, Bellevue, WA) was placed onto the mydriatic eye. Ophthalmoscopically visible marker lesions were used to provide orientation during sample evaluation. Approximately 50 test lesions were placed in 8 columns between the marker lesions in each eye. Ophthalmoscopically visible lesions were placed first and stepwise decreases in power led to invisible laser lesions. Pulse durations of 1 – 200 ms were used, with each column of test lesions corresponding to a single duration.

The animals were sacrificed and eyes were immediately enucleated. Square samples (100 mm^2) were prepared from the posterior segment of each eye and the neural retina was peeled away to expose the RPE. Samples were immediately stained with a solution of Ethidium homodimer 1 (EthD-1), a membrane permeable dye that binds to nucleic acids and undergoes an enhancement of fluorescence [29]. Digital fluorescence images were taken 20 minutes after staining to assess cell viability. Diameter of the damaged zone was measured in each lesion using *ImageJ*.

2.6 Computational model of thermal damage

Axi-symmetric geometries were constructed in COMSOL 3.4 to model laser treatment of porcine RPE explant and *in vivo* rabbit posterior pole [30]. The RPE is the primary absorbing layer in both models, with a high concentration of micrometer-sized melanin granules [15]. During millisecond laser exposures heat diffuses from these granules to tens of micrometers, supporting the assumption of homogeneous pigment distribution inside a cell. The models were thus constructed as series of homogeneous absorbing layers, with a cell-to-cell variability in pigmentation taken into account as described below. The RPE explant model was made up of RPE and choroidal layers, while the rabbit *in vivo* model consisted of five absorbing layers: neural retina, RPE, choriocapillaris, pigmented choroid and non-pigmented choroid.

Heat deposition depends on layer absorption coefficients and beam irradiance distribution. In highly forward-scattering tissue such as retina, axial attenuation of the laser irradiation can be described with a modified Beer-Lambert law and leads to a heat source distribution:

$$Q(r,z) = \mu_a(z) \cdot \Phi(r) \cdot \exp\left[-(\mu_a + (1-g)\mu_s)z\right] \tag{2}$$

where $\Phi(r)$ is the irradiance profile, $\mu_a(z)$ and $\mu_s(z)$ are the layer absorption and scattering coefficients, and g is the anisotropy factor [31, 32]. An error function fit was performed to parameterize measured aerial and in-eye radial irradiance profiles for the *in vitro* and *in vivo* models, respectively:

$$\Phi(r) = \Phi_0\left[erf\left(\frac{a-r}{b}\right)+1\right] \tag{3}$$

where a and b are fit parameters and Φ_0 is the peak irradiance. Layer thicknesses were estimated from histology and literature [16]. Absorption in the RPE was inferred from RPE pigmentation and bulk transmission measurements (Sec. 3.1), while remaining absorption coefficients were taken from literature [15, 33]. Layer thicknesses and beam attenuation properties are summarized in Table 1.

Table. 2. Layer attenuation properties at 532 nm wavelength, determined from literature, histology and experimental measurements [15, 16, 33].

Ocular Tissue	**Thickness Δz (μm)**	**Absorption μ_a (1/cm)**	**Scattering μ_s (1/cm)**	**Anisotropy factor g**	**$(1-g)\mu_s$ (1/cm)**
Porcine *in vitro* model					
RPE	4	1400	1100	0.84	180
Choroid	70	160	740	0.87	96
Rabbit *in vivo* model					
Neural retina	112	4.2	340	0.97	10
RPE	4	1400	1100	0.84	180
Choriocapillaris	20	160	740	0.87	96
Pigmented Choroid	20	1400	740	0.87	96
Non-pigmented Choroid	30	160	740	0.87	96

The time-dependent heat conduction equation was used to describe temperature evolution in the model layers upon laser treatment:

$$\rho c_p \frac{\partial T}{\partial t} = \nabla \cdot (k \nabla T) + Q(r,z,t) \tag{4}$$

where ρ and c_p are the density and heat capacity of the medium, k is the thermal conductivity and Q is the volumetric heat source term described above. Thermal properties of liquid water were used for the modeled tissue [34]. Blood perfusion and other convective cooling processes were not included in the final computations, as they been shown to have only a small effect on temperature rise for millisecond pulse durations [18, 35]. Constant temperature condition was assumed on the external boundaries, while zero heat flux was maintained on the axis of symmetry. The model was 500 µm in radial extent and included 400 µm non-absorbing layers above and below the top and bottom-most absorbing layers to ensure that the computational domain was sufficiently large, and boundary conditions did not have a significant effect.

COMSOL 3.4 was used to define the described geometries and generate finite-element meshes [30]. A direct linear system solver computed solutions to the heat conduction equation with finite-element method. The Arrhenius damage model describes tissue damage as the integral of a temperature-dependent damage rate over a period of temperature elevation [15, 19, 20, 24]. This integral was computed with trapezoidal integration throughout the model using the calculated temperature time-courses. The Arrhenius model parameters E^* and A in these calculations were extracted from computed temperature time-courses corresponding to the RPE viability measurements.

3. RESULTS

3.1 RPE pigmentation

Threshold fits were applied to the RPE transmission micrographs in *ImageJ* to define boundaries of the pigmented cell regions. For each region, mean grayscale value C_{cell} and area were calculated. To quantify cell-to-cell transmission variations, black (wire on sample) and white (missing cell in RPE sheet) reference levels C_{white} and C_{black} were measured and fractional transmission was computed:

$$T_{cell} = \frac{C_{cell} - C_{black}}{C_{white} - C_{black}} \tag{5}$$

Figure 2 shows histograms of the region transmission and area. A mean area of 488 µm^2 and transmission of 0.25 were found, corresponding to a circular diameter of 22 µm and absorption coefficient of 3600 cm^{-1}, assuming a pigmented layer thickness of 4 µm. Homogeneous attenuation was calculated from the average fractional transmission over the entire RPE sheets within each image. This gave a transmission of 0.51 ± 0.06, or absorption coefficient of 1700 ± 300 cm^{-1}. For comparison, transmission of the collimated treatment beam through the same samples was 0.60 ± 0.08, or absorption coefficient of 1300 ± 300 cm^{-1}. As the irradiation geometry in this second case was much closer to experimental conditions, bulk RPE absorption was weighted more heavily toward this measurement and an RPE absorption coefficient of 1400 cm^{-1} was used in COMSOL computations. A single cell of diameter 22 µm takes up approximately 2% of irradiated cells in a 200 µm diameter beam. On average, one "hotspot" cell within the beam diameter will have an absorption coefficient corresponding to the lowest 2% of the transmission value histogram, or 5900 cm^{-1}, taking into account scattering attenuation (Table 1).

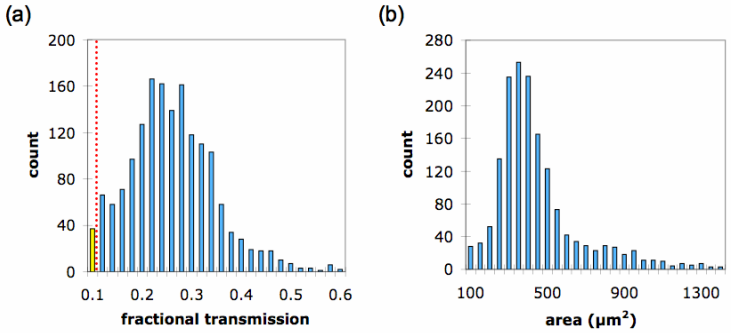

Fig. 2. Transmission (a) and area (b) histograms of fitted pigmented RPE regions. The smallest 2% of transmission values correspond to the "hotspot" central region used in the model and are noted by the vertical line in (a).

3.2 Vaporization delay measurements

Measured delays before vaporization in porcine RPE explant for six laser powers are shown in Figure 3a. An approximate inverse-square-root dependence of power on duration is observed, in agreement with previous measurements *in vivo* [10]. These time delays and powers were used with the computational RPE explant model to provide the expected peak temperatures at vaporization (Fig. 3b). The addition of a central, 11 µm radius "hotspot" to the model RPE layer with absorption coefficient $\alpha_{hotspot}$ = 5900cm^{-1} raises the short duration peak temperature, changing the shape of the peak temperature curve from anomalously increasing with longer duration to remaining relatively constant near 190ºC.

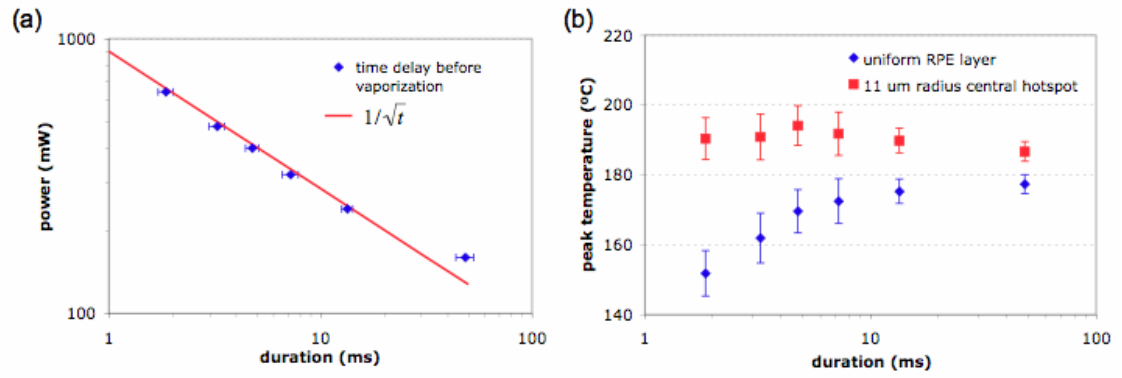

Fig. 3. (a) Laser power required for vaporization at measured time delay. (b) Computed temperatures associated with power/duration pairs (blue) in the uniform absorption model of RPE explant. . With the introduction of a central 22 µm diameter "hotspot" region of higher absorption in the RPE (red), peak temperature is roughly constant with duration.

3.3 Beam characteristics and vaporization modeling in the eye

Figure 4a shows a best-fit error function (eqn. 3) irradiance cross-section for the measured beam in the retinal plane and the expected profile from the aerial beam assuming 0.66× demagnification corresponding to the combined magnifications of the contact lens and rabbit eye [36]. The measured beam is roughly 25% smaller than expected, with a slower taper (22 µm for a 30-70% transition rather than 16 µm). 78% of corneal power was incident on the retina, but only 40% was measured within a 500 µm diameter retinal area, an indication of substantial scattering in the transparent ocular tissues. The cross-sectional fit and measured retinal power were incorporated into the *in vivo* computational model and used to predict temperatures at rupture from the previously measured threshold power data [10]. Peak temperatures are constant around 180 ºC when the measured beam characteristics are included, but temperatures computed for a 0.66× de-magnified aerial beam fit, and no losses in the transparent tissues are of unreasonable magnitude and anomalously increasing with longer exposures.

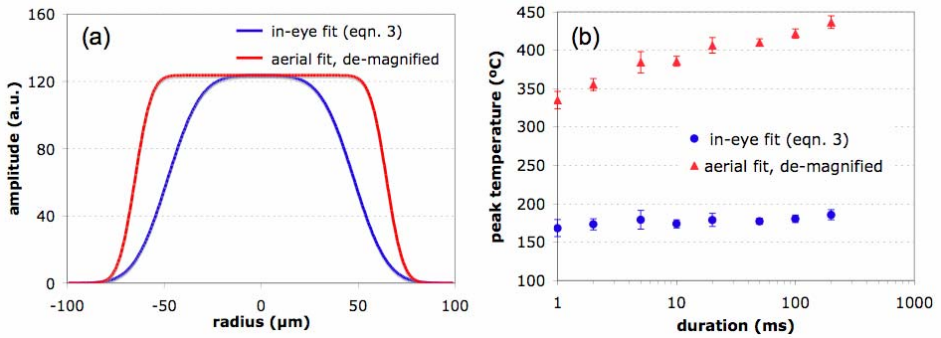

Fig. 4. (a) Fit cross-section of the measured in-eye beam (blue) from eqn. 3 and 0.66x de-magnified aerial beam (red). (b) Computed temperatures at rupture in the rabbit *in vivo* model corresponding to data from

[10]. Temperatures for aerial beam shape with nominal retinal power are shown in red, while those corresponding to the measured beam shape and adjusted retinal power are shown in blue.

3.4 RPE viability measurements

Inset in Figure 5 is a sample fluorescence image from the RPE viability threshold dataset. A threshold lesion diameter (geometric mean of vertical and horizontal widths) of 50 µm was used, and the power to produce threshold lesions at 1 – 200 ms pulse duration was recorded.

The RPE viability data was used as an input to the Arrhenius model of tissue damage. The temperature at the top of the RPE layer at a radius of 25 µm was evaluated and temporal temperature traces were generated. With these traces, damage integrals can be calculated assuming a constant activation energy E* at each duration. E* can be varied, and the least-squares method can be used to find a value giving a constant damage integral value for all power/duration pairs. In this way, a value of E* = 340 ± 40 kJ/mol (3.5 ± 0.4 eV) was obtained and a corresponding rate constant yielding an Arrhenius integral value $\Omega = 1$ was determined to be $A = 1.6\times10^{55}$ s^{-1}..

Figure 5 shows peak computed temperatures at a 25 µm radius associated with the measured threshold powers. The solid line represents the Arrhenius fit, depicting the peak temperatures needed to give an Arrhenius value of exactly unity with the same normalized temporal temperature evolution.

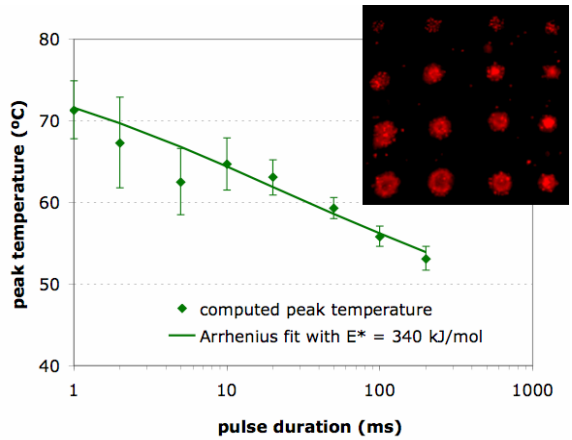

Fig. 5. RPE cell damage threshold temperature as a function of pulse duration. Solid line is an Arrhenius model fit with activation energy of 340 kJ/mol. Inset: Micrograph of RPE sheet with circular lesions containing damaged cells fluorescing in red. Power increases from top to bottom in the image.

3.5 Computed and histological lesion diameters

With a complete thermal damage model, the extent of retinal damage can be predicted for arbitrary laser parameters. Sizes of acute retinal photocoagulation lesions for 10 – 100 ms pulse durations [10] were analyzed histologically, and compared with model predictions. A sample histological section with overlaid corresponding temperature map and the damage zone boundary ($\Omega = 1$) are shown in Figure 6a. Histological damage zone was defined by abnormal appearance of the RPE and photoreceptor outer segments. Corresponding laser parameters were used as input to the *in vivo* computational model, and the width of the computed damage zone was defined as the diameter of the damage contour at the top of the RPE layer.

Experimental (symbol) and computed (solid line) lesion diameters are plotted in Figure 6b as a function of duration and laser power. Damage zone width follows a logarithmic dependence on duration and is roughly linear with power. The degree of quantitative agreement between histological and computed lesion diameters indicates that the retinal coagulation model has predictive capabilities.

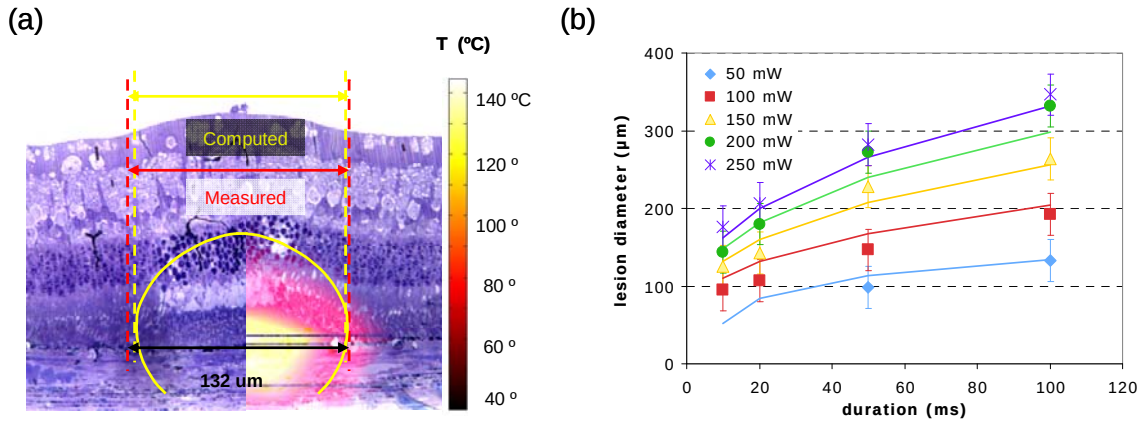

Fig. 6. (a) Peak temperature in tissue and circumference of the cellular damage zone (yellow contour) computed by the thermal model for 10 ms, 150 mW pulse, overlaid on a corresponding histological section. (b) Modeled (solid line) and histological (symbol) measurements of lesion width as a function of pulse duration and laser power for a 200 µm aerial beam diameter. Error bars give conservative estimates of the uncertainty in the measured lesion width.

4. DISCUSSION

4.1 RPE heating and vaporization

A critical parameter determining absolute temperature in the computational model is the absorption in the pigmented layers, especially in the RPE. The homogeneous absorption coefficient of RPE used in the model (1400 cm^{-1}) and the measured fractional absorption (40 ± 8%) in RPE sheath both fall in the ranges typically assumed in thermal modeling of visible laser treatment of the retina [15, 33, 37, 38]. The inhomogeneous deposition of heat in the RPE was found to be very important, particularly in the estimation of vaporization thresholds. A central 22 µm hotspot modeling the non-uniformity in RPE pigmentation was necessary to yield a reasonably constant temperature (~190 ºC) at vaporization threshold across the millisecond time range. Fundus pigmentation variations due to changes in melanosome density have been previously reported and noted as a possible reason for observed variations in photocoagulation outcomes [39, 40].

Vaporization in the RPE has been studied for microsecond and nanosecond laser pulses, where heat is confined to melanosomes, and melanosome surface temperature at vaporization has been estimated to be 157 ± 33 ºC [41]. For millisecond pulses, temperature distribution across the RPE cell is near-uniform due to heat diffusion, but bubbles are expected to continue nucleating around melanosomes. The *in vivo* and *in vitro* vaporization threshold temperatures computed in this work (168 – 192 ºC) for millisecond pulses fall within the temperature range previously estimated for microsecond pulses [41].

In addition to RPE absorption variations, beam shape and ocular power transmission were also found to be important for accurate modeling of retinal heating. Greater beam demagnification (0.53×) was observed than expected (0.66×), and radial taper was 27% slower than the de-magnified aerial beam, though the top-hat shape was well preserved. The measured ocular transmittance of 78% is comparable to previous estimations by Kidwell et al. [42], and the fractional power transmittance within the focal spot (40%) agrees with other estimations [43]. The measured power transmission to the focus may be due to scattering in the anterior segment, lens and vitreous, though the origin of the scattering remains to be investigated. Taking into account the actual beam characteristics was essential to yield a constant temperature value near the vaporization threshold measured in-vitro and in-vivo.

4.2 Cellular viability

Measured RPE viability threshold radiant exposures for 1 – 200 ms pulses were 1.2 – 25 J/cm^2, in agreement with previous comparable measurements in bovine and porcine explants [13, 21]. These thresholds corresponded to computed temperatures falling from 72 ºC at 1 ms to 53 ºC at 200 ms. Threshold temperatures from long-duration cellular hyperthermia experiments have been estimated in the range of 40 – 55 ºC [44, 45]. Direct *in vivo* retinal temperature measurements of 92 – 62ºC for 20 ms – 10 s pulses during photocoagulation have been reported [46]. These measurements corresponded to visible lesions, which are expected to have threshold powers approximately 2× higher than the RPE viability threshold. Thermal damage is known to be the mechanism for RPE death for millisecond duration pulses [21, 47], and the Arrhenius model has been applied to retinal tissue in previous studies [13-15]. The activation energy E* reported here (340 kJ/mol = 3.5 eV) is comparable to that of Vassiliadis (290 kJ/mol = 3.0 eV) [27].

Validation of the computational model was based on a comparison of the predicted damage zone with histological measurements (Fig. 6b). Radial damage extent at the RPE showed quantitative agreement between model and histology over a wide range of laser parameters. Histological lesion diameter appears to vary logarithmically with duration and linearly with power, trends previously observed for ophthalmoscopic lesion width [10].
Accurate retinal damage modeling can have immediate clinical relevance. In comparing efficacy of different photocoagulation treatment parameters, it is desirable to adjust the number of lesions to maintain a constant coagulated retinal area. This can be facilitated by lesion size calculations with a computational model.

4.3 Increasing the therapeutic window

Optimization of the beam shape for improvement of the safety of retinal photocoagulation is another important application for computational modeling. With conventional top-hat beams and millisecond pulse durations, heat diffusion results in a central region of higher temperature, increasing the probability of rupture. A beam with lower central intensity could give a more uniform temperature profile and wider therapeutic window.

To quantify possible improvement, a ring-shaped beam was implemented in the *in vivo* model. The Laguerre-Gaussian LP01* transverse mode of a multimode optical fiber was used, which has a radial profile:

$$\Phi(r) = \Phi_0 \frac{r^2}{w^2} e^{-2\frac{r^2}{w^2}} \tag{12}$$

where w is the Gaussian width. The threshold powers for the ring beam were computed to produce the same lesion width at 1 – 200 ms pulse duration as with the conventional top-hat beam. Rupture threshold was calculated as the power required for a peak temperature of 180 ºC. The ratio of these computed thresholds gave the therapeutic window for the ring beam (Fig. 7), which showed roughly 2× improvement over *in vivo* measurements at durations less than 10 ms. The improved safety predicted for the ring beam may be clinically important: pulse durations down to 2 ms can be considered safe with such a beam, rather than 20 ms limit with a conventional beam. This decrease in pulse duration would allow for a 10× more lesions to be applied in a single pattern and would further improve confinement of the thermal effects in the retina.

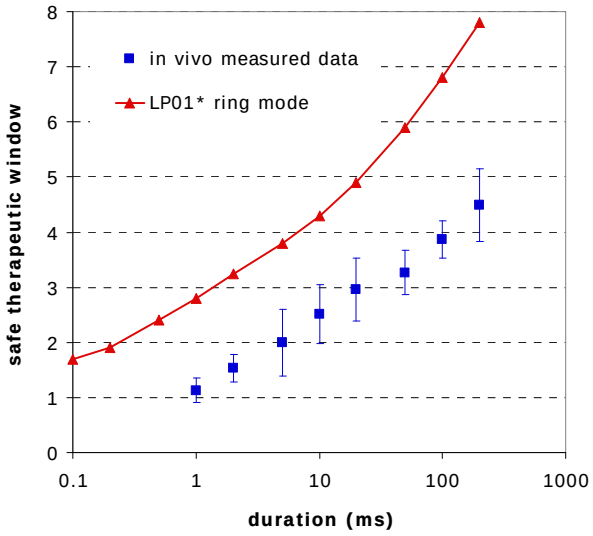

Fig. 7. Computed therapeutic window (TW), the ratio of threshold powers for rupture and light coagulation, with a ring beam (red) and measured *in vivo* data (blue) [10]. Safe TW is generally considered to be greater than 3.

5. CONCLUSIONS

A computational retinal photocoagulation model has been constructed based on experimentally verified absorption characteristics of ocular tissues, as well as thresholds of RPE damage, retinal coagulation and rupture. Variability in RPE pigmentation was found to play a very significant role in calculating temperature at rupture. An Arrhenius damage model with activation energy of 340 kJ/mol matched the RPE viability thresholds, and predicted the retinal damage zone widths that matched histological findings. Ring-shaped beams are expected to substantially improve safety at short durations (2 – 20 ms). Future studies aim to verify this expected increase experimentally, and compute optimal treatment parameters for millisecond photocoagulation.

ACKLOWLEDGEMENTS

The authors thank Roopa Dalal, Georg Schuele and Nathan Palanker for laboratory assistance. Funding was provided by US Air Force Office of Scientific Research (MFEL Program) and Stanford Photonics Research Center (SPRC).

REFERENCES

1. H. L. Little, H. C. Zweng and R. R. Peabody, "Argon laser slit-lamp retinal photocoagulation," Trans Am Acad Ophthalmol Otolaryngol 74(1), 85-97 (1970)
2. "Treatment techniques and clinical guidelines for photocoagulation of diabetic macular edema. Early Treatment Diabetic Retinopathy Study Report Number 2. Early Treatment Diabetic Retinopathy Study Research Group," Ophthalmology 94(7), 761-774 (1987)
3. "The influence of treatment extent on the visual acuity of eyes treated with Krypton laser for juxtafoveal choroidal neovascularization. Macular Photocoagulation Study Group," Arch Ophthalmol 113(2), 190-194 (1995)
4. N. S. Kapany, et al., "Retinal Photocoagulation by Lasers," Nature 199(146-149 (1963)
5. M. A. Mainster, "Decreasing retinal photocoagulation damage: principles and techniques," Seminars in Ophthalmology 14(4), 200-209 (1999)

6. M. S. Blumenkranz, D. Yellachich, D. E. Andersen, M. W. Wiltberger, D. Mordaunt, G. R. Marcellino and D. Palanker, "Semiautomated patterned scanning laser for retinal photocoagulation," Retina 26(3), 370-376 (2006)
7. S. Al-Hussainy, P. M. Dodson and J. M. Gibson, "Pain response and follow-up of patients undergoing panretinal laser photocoagulation with reduced exposure times," Eye 22(1), 96-99 (2008)
8. J. Roider, F. Hillenkamp, T. Flotte and R. Birngruber, "Microphotocoagulation - Selective Effects of Repetitive Short Laser-Pulses," P Natl Acad Sci USA 90(18), 8643-8647 (1993)
9. A. Obana, "The therapeutic range of chorioretinal photocoagulation with diode and argon lasers: an experimental comparison," Lasers and Light in Ophthalmology 4(3/4), 147-156 (1992)
10. A. Jain, M. S. Blumenkranz, Y. Paulus, M. W. Wiltberger, D. E. Andersen, P. Huie and D. Palanker, "Effect of pulse duration on size and character of the lesion in retinal photocoagulation," Arch Ophthalmol 126(1), 78-85 (2008)
11. S. Schmidt and R. Peisch, "Melanin concentration in normal human retinal pigment epithelium. Regional variation and age-related reduction," Invest. Ophthalmol. Vis. Sci. 27(7), 1063-1067 (1986)
12. J. Weiter, F. Delori, G. Wing and K. Fitch, "Retinal pigment epithelial lipofuscin and melanin and choroidal melanin in human eyes," Invest. Ophthalmol. Vis. Sci. 27(2), 145-152 (1986)
13. K. Schulmeister, J. Husinsky, B. Seiser, F. Edthofer, H. Tuschl and D. J. Lund, "Ex-plant retinal laser induced threshold studies in the millisecond time regime," in Optical Interactions with Tissue and Cells XVII S. L. Jacques and W. P. Roach, Eds., p. 60841E, SPIE (2006).
14. A. J. Welch, "The Thermal Response of Laser Irradiated Tissue," Ieee Journal of Quantum Electronics 20(12), 1471-1481 (1984)
15. R. Birngruber, F. Hillenkamp and V. P. Gabel, "Theoretical Investigations of Laser Thermal Retinal Injury," Health Physics 48(6), 781-796 (1985)
16. J. Sandeau, G. Caillibotte, J. Kandulla, R. Birngruber and G. Apiou-Sbirlea, "Modeling of conductive and convective heat transfers in retinal laser treatments," in Ophthalmic Technologies XVI F. Manns, P. G. Soderberg and A. Ho, Eds., p. 61381A, SPIE (2006).
17. C. R. Thompson, B. S. Gerstman, S. L. Jacques and M. E. Rogers, "Melanin granule model for laser-induced thermal damage in the retina," Bull Math Biol 58(3), 513-553 (1996)
18. R. K. Banerjee, L. Zhu, P. Gopalakrishnan and M. J. Kazmierczak, "Influence of laser parameters on selective retinal treatment using single-phase heat transfer analyses," Medical Physics 34(5), 1828-1841 (2007)
19. F. C. Henriques and A. R. Moritz, "Studies of Thermal Injury in the Conduction of Heat to and through Skin and the Temperatures Attained Therein - a Theoretical and an Experimental Investigation," Am J Pathol 23(4), 915-934 (1947)
20. J. P. a. S. Thomsen, "Rate process analysis of thermal damage," in Optical-Thermal Response of Laser-Irradiated Tissue A. J. W. a. M. J. C. v. Gemert, Ed., pp. 561-603, Plenum, New York (1995).
21. G. Schuele, M. Rumohr, G. Huettmann and R. Brinkmann, "RPE damage thresholds and mechanisms for laser exposure in the microsecond-to-millisecond time regimen," Invest Ophthalmol Vis Sci 46(2), 714-719 (2005)
22. R. Brinkmann, G. Huttmann, J. Rogener, J. Roider, R. Birngruber and C. P. Lin, "Origin of retinal pigment epithelium cell damage by pulsed laser irradiance in the nanosecond to microsecond time regimen," Lasers in Surgery and Medicine 27(5), 451-464 (2000)
23. P. W. Lappin and P. S. Coogan, "Relative sensitivity of various areas of the retina to laser radiation," Arch Ophthalmol-Chic 84(3), 350-354 (1970)
24. M. Niemz, Laser-Tissue Interactions. Fundamentals and Applications, Springer, Berlin (2002).
25. D. M. Simanovskii, M. A. Mackanos, A. R. Irani, C. E. O'Connell-Rodwell, C. H. Contag, H. A. Schwettman and D. V. Palanker, "Cellular tolerance to pulsed hyperthermia," Phys Rev E Stat Nonlin Soft Matter Phys 74(1 Pt 1), 011915 (2006)
26. J. Kampmeier, B. Radt, R. Birngruber and R. Brinkmann, "Thermal and biomechanical parameters of porcine cornea," Cornea 19(3), 355-363 (2000)
27. A. Z. Vassiliadis, H. Christian ; Dedrick, Kent G., "Ocular Laser Threshold Investigations," in SRI Proj. 8209, Stanford Research Institute Menlo Park California (1971).
28. W. Rasband, "ImageJ," U.S. National Institutes of Health, Bethesda, MD (2004).
29. Invitrogen, "LIVE/DEAD (R) Viability/Cytotoxicity Kit, Data Sheet, http://www.invitrogen.com/," (2005).
30. "COMSOL Multiphysics 3.4," COMSOL Inc. (http://www.comsol.com/) (2007).

31. M. J. C. Vangemert and J. P. H. Henning, "A Model Approach to Laser Coagulation of Dermal Vascular-Lesions," Arch Dermatol Res 270(4), 429-439 (1981)
32. P. Kubelka, "New Contributions to the Optics of Intensely Light-Scattering Materials .1.," J Opt Soc Am 38(5), 448-457 (1948)
33. M. Hammer, A. Roggan, D. Schweitzer and G. Muller, "Optical properties of ocular fundus tissues-an in vitro study using the double-integrating-sphere technique and inverse Monte Carlo simulation," Physics in Medicine and Biology 40(6), 963-978 (1995)
34. "The International Association for Properties of Water and Steam (IAPWS), "Revised Release on the IAPS Formulation 1985 for the Thermal Conductivity of Ordinary Water Substance for General and Scientific Use"," (1998).
35. A. J. Welch, E. H. Wissler and L. A. Priebe, "Significance of Blood-Flow in Calculations of Temperature in Laser Irradiated Tissue," Ieee T Bio-Med Eng 27(3), 164-166 (1980)
36. R. Birngruber, "Choroidal circulation and heat convection at the fundus of the eye: implications for laser coagulation and the stabilization of retinal temperature," in Laser Applications to Medicine and Biology M. L. Wolbarsht, Ed., p. 277–361, Plenum Press, London (1991).
37. G. Schule, G. Huttmann, C. Framme, J. Roider and R. Brinkmann, "Noninvasive optoacoustic temperature determination at the fundus of the eye during laser irradiation," J Biomed Opt 9(1), 173-179 (2004)
38. V. P. Gabel, Birngruber R, Hillenkamp F., "Visible and near infrared light absorption in pigment epithelium and choroid.," Congress Series: XXIII Concilium Ophthalmologicum 450(658-662 (1978)
39. J. S. Pollack, J. E. Kim, J. S. Pulido and J. M. Burke, "Tissue Effects of Subclinical Diode Laser Treatment of the Retina
10.1001/archopht.116.12.1633," Arch Ophthalmol 116(12), 1633-1639 (1998)
40. M. F. Marmor and T. J. Wolfensberger, The retinal pigment epithelium : function and disease, New York : Oxford University Press, 1998 (1998).
41. J. Neumann and R. Brinkmann, "Boiling nucleation on melanosomes and microbeads transiently heated by nanosecond and microsecond laser pulses," J Biomed Opt 10(2), 024001 (2005)
42. T. P. Kidwell, L. A. Priebe and A. J. Welch, "Measurement of Ocular Transmittance and Irradiation Distribution in Argon-Laser Irradiated Rabbit Eyes," Investigative Ophthalmology 15(8), 668-671 (1976)
43. R. Birngruber, E. Drechsel, F. Hillenkamp and V.-P. Gabel, "Minimal spot size on the retina formed by the optical system of the eye," International Ophthalmology 1(3), 175-178 (1979)
44. S. Bhowmick, J. E. Coad, D. J. Swanlund and J. C. Bischof, "In vitro thermal therapy of AT-1 Dunning prostate tumours," International Journal of Hyperthermia 20(73-92 (2004)
45. J. R. Lepock, "Cellular effects of hyperthermia: relevance to the minimum dose for thermal damage," International Journal of Hyperthermia 19(252-266 (2003)
46. L. A. Priebe, C. P. Cain and A. J. Welch, "Temperature Rise Required for Production of Minimal Lesions in Macaca-Mulatta Retina," American Journal of Ophthalmology 79(3), 405-413 (1975)
47. H. Lee, C. Alt, C. M. Pitsillides and C. P. Lin, "Optical detection of intracellular cavitation during selective laser targeting of the retinal pigment epithelium: dependence of cell death mechanism on pulse duration," J Biomed Opt 12(6), 064034 (2007)